

Stationary crack propagation in a two-dimensional visco-elastic network model

Yuko Aoyanagi, Ko Okumura*

Department of Physics and Soft Matter Center, Ochanomizu University, 2-1-1, Otsuka, Bunkyo-ku, Tokyo 112-8610, Japan

Abstract

We investigate crack propagation in a simple two-dimensional visco-elastic model and find a scaling regime in the relation between the propagation velocity and energy release rate or fracture energy, together with lower and upper bounds of the scaling regime. On the basis of our result, the existence of the lower and upper bounds is expected to be universal or model-independent: the present simple simulation model provides generic insight into the physics of crack propagation, and the model will be a first step towards the development of a more refined coarse-grained model. Relatively abrupt changes of velocity are predicted near the lower and upper bounds for the scaling regime and the positions of the bounds could be good markers for the development of tough polymers, for which we provide simple views that could be useful as guiding principles for toughening polymer-based materials.

Keywords: fracture, crack propagation, visco-elasticity

1. Introduction

Polymer-based materials are widely used for industrial products and developing tough polymers are significantly important for our life. Given that material toughness is governed by cracks at the tips of which stress is concentrated [1, 2],

*Corresponding author

Email address: okumura@phys.ocha.ac.jp (Ko Okumura)

5 crack propagation in polymer-based materials should be a subject of wide in-
terest for researchers in academia as well as those in industry. In fact, fracture
energy required for crack propagation and its dependence on the propagation
speed have been studied for various polymer-based materials, such as adhesive
interface [3, 4, 5, 6], flexible laminates [7], viscoelastic solids [8, 9, 10, 11, 12],
10 weakly crosslinked gels [13, 14], and soft polymer foam [15]. In the case of
viscoelastic materials, such as rubbers and elastomers, a simple scaling regime
has been shown experimentally [4, 12] in the relation between the fracture en-
ergy and velocity when viscoelasticity dominates the fracture energy (note that
rapid crack propagations are strongly affected by inertia [16, 17, 18] and that the
15 greatest lower bound for the scaling regime has been discussed in the literature
[19, 20]). This scaling law has been discussed theoretically using frameworks
based on linear viscoelasticity and linear fracture mechanics by three different
groups [9, 10, 11] and, although the near-crack treatments are different among
the groups, they all concluded essentially the same scaling law in a high veloc-
20 ity limit, suggesting the importance of the far-field contribution coming from
viscoelastic dissipation occurring at regions remote from crack tips [21].

However, the complete physical picture for the far-field viscoelastic regime
has yet to be clarified with lack of any coarse-grained simulation models for the
problem. We study the crack propagation in a lattice model that incorporates a
25 linear viscoelasticity in a simple manner. The use of lattice model is motivated
by the previous theories [9, 10, 11], in which the dynamics originating from the
far-field linear viscoelastic contribution are fairly insensitive to near-crack treat-
ments. As a result, we reproduce crack propagation with a constant velocity.
In addition, we find that the velocity as a function of fracture energy or energy
30 release rate exhibits a scaling regime similar to the one discussed in experimen-
tal studies [4, 22, 23]. Furthermore, we find that there are a lower bound [19]
and an upper bound [24] for the scaling regime, and we draw simple physical
interpretations for the bounds. Since the interpretations are independent of the
details of the model, the present simulation model provides generic insight into
35 the physical understanding of the crack propagation, which may be helpful for

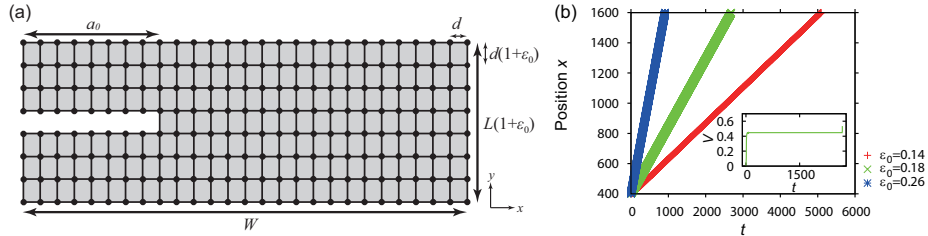


Fig. 1: (a) Two-dimensional network at the start of simulation. (b) Position of crack tip x vs time t for three different initial strains ε_0 for $(E, \eta, \varepsilon_c, d, L) = (100, 80, 0.35, 1, 200)$. The inset shows the relation between crack speed V vs t at the initial strain $\varepsilon_0 = 0.18$.

the development of tough polymer materials.

2. Simulation model

In the simulations performed in the present study, we prepare a two-dimensional square-lattice system with the lattice constant d as shown in Fig. 1(a). The width and height are W and L , respectively. Before starting a simulation, we prepare an equilibrium state of the network with a homogeneous strain ε_0 by applying fixed displacements at the top and bottom of the system. The edge displacements are fixed during the simulation (fixed-grip condition). The simulation is initiated by introducing a crack of the initial length a_0 by cutting
 40 (i.e. removing) the corresponding elastic bonds as illustrated in Fig. 1(a). The parameters (W, a_0) are fixed to $(1600, 400)$ throughout this work in the unit length specified below.
 45

The lattice dynamics is determined by the following mechanism. Each bead in the lattice feels elastic force from the four nearest neighbors (except for the beads at the edges), whereas viscous force acts on each bead. Since we are interested in a purely viscoelastic regime, we neglect the inertia of each bead. The dynamics of the simulation model can be characterized by the following equation:

$$k\Delta x_{i,j} = -\eta\dot{x}_{i,j} \quad (1)$$

where k and η are the spring constant and viscosity, respectively. Here, $x_{i,j}$

stands for the vertical position of the bead located originally at the lattice point
 50 (i, j) and $\dot{x}_{i,j}$ is the time derivative of $x_{i,j}$. The quantity $\Delta x_{i,j}$ stands for the
 local displacement, defined as the sum of the elongation of the four bonds (or
 springs) connecting the lattice point (i, j) to the four nearest-neighbor lattice
 points $x_{i,j}^{(s)}$ ($s = 1, \dots, 4$): $\Delta x_{i,j}$ is given by $\Delta x_{i,j} = \sum_{s=1}^4 (x_{i,j}^{(s)} - x_{i,j} - \ell^{(s)})$ with
 the natural length $\ell^{(s)}$ of the springs with $\ell^{(1)} = \ell^{(3)} = 0$ and $\ell^{(2)} = \ell^{(4)} = d$
 55 ($s = 1$ and 3 correspond to shear and $s = 2$ and 4 correspond to stretch) [25].
 In order for a crack to propagate, every spring is broken when the force acting
 on it reaches the critical value f_c .

For later convenience, we define the local “strain” and “stress” $\varepsilon \equiv \Delta d/d$ and
 $\sigma \equiv f/d^2 = E\varepsilon$ with the “elastic modulus” $E \equiv k/d$. Here, Δd is the elongation
 60 of a bond and f is the force acting on the bond. Given that there is extensive
 literature on lattice modelling where relations between lattice parameters and
 the material Young’s modulus and Poisson’s ratio are discussed (e.g. [26, 27]),
 it is clear that our results cannot be directly compared with experiment through
 the “strain” and “stress” defined above. However, this work discusses fracture
 65 mechanical concepts, which are based on continuum theory, and we do not
 aim at relating our “stress” and “strain” to measurable macroscopic properties
 but rather aim at providing physical scenario emerging from a simple model.
 Accordingly, we use the above definition, which is dimensionally correct and
 useful to greatly simplify the introduction and discussion of quantities that
 70 appear in the fracture mechanical context. With the same spirit, we define σ_c
 by $f_c = \sigma_c d^2$ with $\sigma_c = E\varepsilon_c$ and the principal relaxation time τ by $\tau = \eta/E$.

The units are specified by the fundamental units of length l_0 , elasticity E_0 ,
 and viscosity η_0 , which are all set to one, in the simulations (for example, the
 units of time and velocity are given by $\tau_0 = \eta_0/E_0$ and $V_0 = l_0/\tau_0$, respectively).

75 The creep dynamics of the present model is similar to that of the Kelvin-
 Voigt model: under a constant stress, the strain slowly increases with time and
 finally reaches a constant value. In fact, the present model possesses N different
 relaxation times with $N = L/l_0$. The details of rheological properties of the
 simple model will be discussed elsewhere.

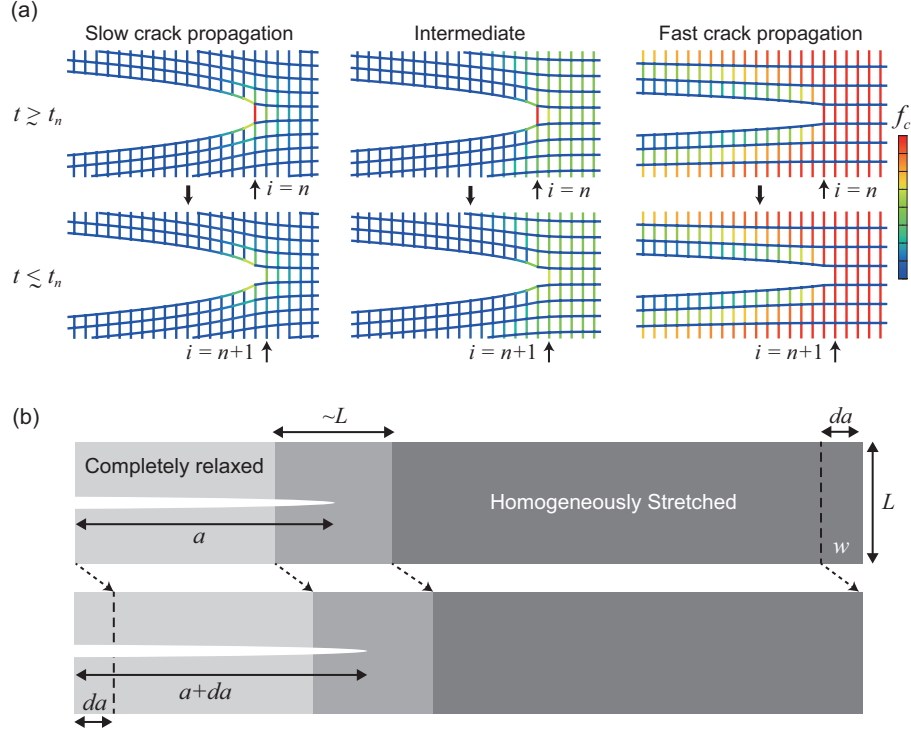


Fig. 2: (a) The states just before and after the bond breaking at the crack tip are shown for slow crack propagation at $\varepsilon_0 = 0.070$ (left) and fast propagation at $\varepsilon_0 = 0.345$ (right), for the same parameter set as in Fig. 1(b). The middle is obtained at $\varepsilon_0 = 0.20$, i.e., at a velocity in the middle of the scaling regime shown in Fig. 3 below. (b) Illustration of the elastic field in the system.

80 3. Results

3.1. Crack propagation with a constant speed

We confirmed that the crack expands with a constant speed for all the parameters we investigated as demonstrated in Fig. 1(b). As shown in the inset, after a short transient regime, the crack propagation velocity reaches a constant
85 value V . Figure 2(a) demonstrates that the crack tip shape changes with speed, which is further discussed in Sec. 4.

3.2. Fracture energy vs crack propagation speed

In the present simulations, the energy release rate during the constant-speed crack propagation is identified with the initially stored elastic energy multiplied by the system height:

$$G = wL = \frac{1}{2}E\varepsilon_0^2L \quad (2)$$

where w is the density of the initial elastic energy $E\varepsilon_0^2/2$. This is because, as shown in Fig. 2(b), in the left (right) region away from the crack tip by the distance $\sim L$, the elastic field is completely relaxed (the elastic field is homogeneous with the initial energy density w) [28]. Note that G is defined by $G = -dU/dA$ with U the elastic potential energy and A the fracture surface. In the present case, G can be interpreted as a velocity-dependent fracture energy since this rate has the meaning of the energy required to create a unit area of fracture surface at a given speed.

As demonstrated below, the results of simulation show that, when V/V_0 is plotted as a function of G/G_0 , all the simulation data collapse on to a master curve, which can be characterized reasonably well by the following scaling law

$$\frac{V}{V_0} \simeq \left(\frac{G}{G_0}\right)^\nu \quad \text{for } \frac{d}{L} \ll \frac{G}{G_0} \ll 1 \quad (3)$$

where the exponent ν is approximately one, with relatively abrupt changes in velocity at the both ends ($G/G_0 \simeq d/L$ and $G/G_0 = 1$) of the scaling regime. These abrupt changes imply that the master curve diverges in the upper limit and converges to zero in the lower limit. Here, we have introduced natural units of the rate G_0 and the velocity V_0 :

$$G_0 = w_c L \quad \text{with } w_c = \frac{1}{2}E\varepsilon_c^2 \quad \text{and } V_0 = \frac{d}{\tau} \quad (4)$$

In Fig. 3, the crack propagation speed V is given as a function of the energy release rate G during the crack propagation for various parameters (E, η, ε_c) with fixed (d, L). In Fig. 4, V is given as a function of G for various parameters (d, L) with fixed (E, η, ε_c). In both cases, when the velocity and the energy release rate G are renormalized by the natural units V_0 and G_0 given in Eq.

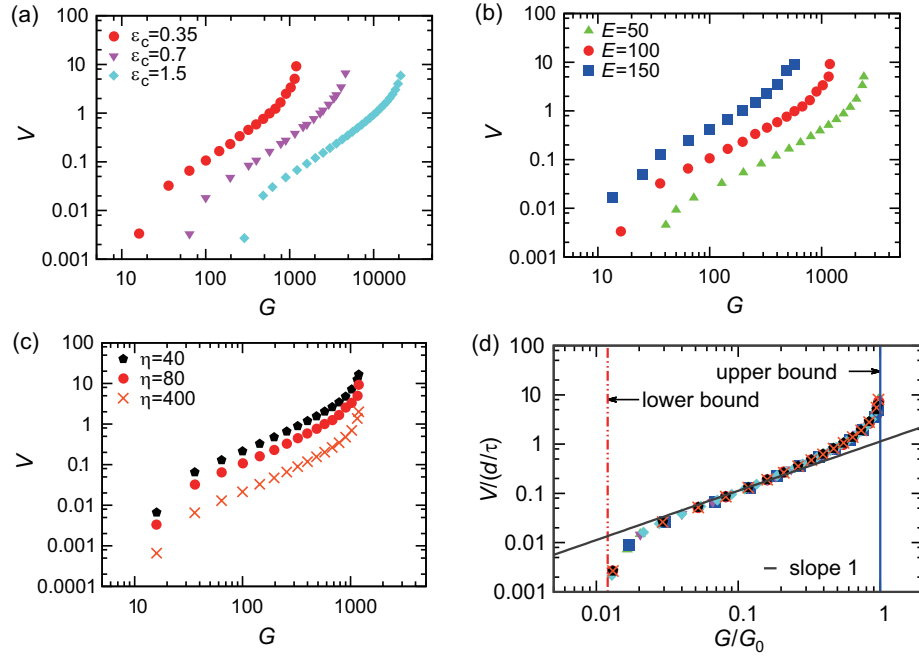


Fig. 3: Crack propagation speed V vs. energy release rate G for different values of (a) ε_c with $(E, \eta) = (100, 80)$, (b) E with $(\eta, \varepsilon_c) = (80, 0.35)$ and (c) η with $(E, \varepsilon_c) = (100, 0.35)$, where (d, L) is fixed to $(1, 200)$. (d) $V/(d/\tau)$ vs G/G_0 . The value of d/L in all the cases is $1/200$ and the vertical dashed line indicating the lower bound corresponds to $G/G_0 = k_1 d/L$ with $k_1 = 2.4$.

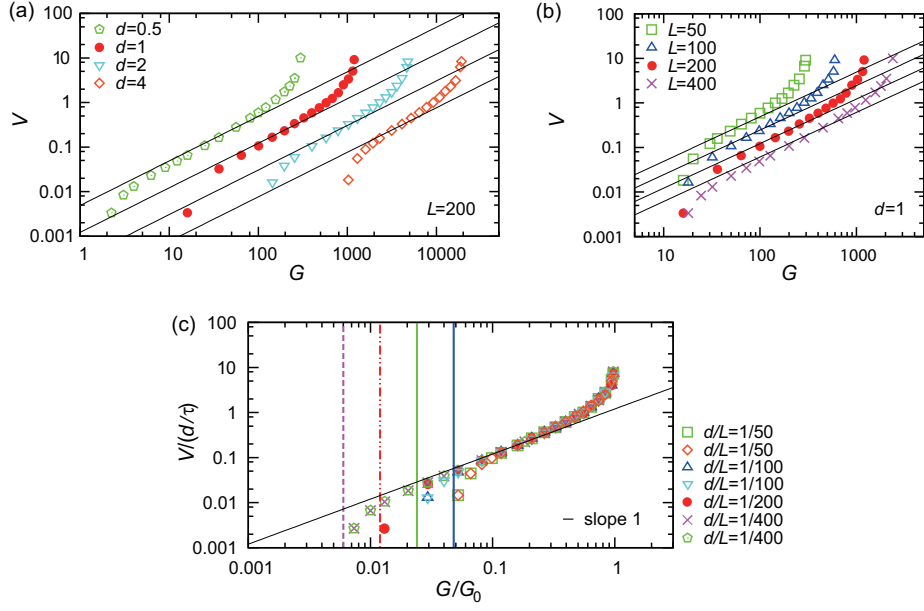


Fig. 4: Crack propagation speed V vs. energy release rate G for different values of (a) d with $L = 200$ and (b) L with $d = 1$, where $(E, \eta, \varepsilon_c) = (100, 80, 0.35)$. (c) $V/(d/\tau)$ vs G/G_0 . Four straight lines in (a) and those in (b) correspond to the straight line with slope 1 in (c). In (a) and (b), seven sets of the data with different (d, L) are distinguished by seven different symbols; the data set represented by the filled circles (red circles on the web version) obtained for $d = 1$ and $L = 200$ is shown in both (a) and (b). These seven sets of data are shown in (c) with using the same symbols. The four vertical lines indicating the lower bounds for four different values of d/L correspond to $G/G_0 = k_1 d/L$ with $k_1 = 2.4$.

(4), all the data are superposed as in Fig. 3(d) and Fig. 4(c), suggesting a linear scaling regime characterized by the straight line with slope one and the existence of the lower and upper bounds for the scaling regime with the upper bound $G/G_0 = 1$. We further confirmed numerically that the lower bound is proportional to d/L in Fig. 4(c) (this is shown by the fact that the four vertical lines showing the lower bounds for different d/L are equally spaced), which is theoretically justified by the arguments in Sec. 4.3.

Some of the exponents in the scaling regions in Figs. 3 and 4 are given numerically as follows. As suggested above, the scaling regime becomes wider as d/L gets smaller, we select from Fig. 4 the data with the smallest to third smallest values of d/L ($d/L = 1/400, 1/200$ and $1/100$) and numerically obtained the exponents, which are respectively given as 1.13, 1.23 and 1.25. (The exponent is obtained numerically by fitting a straight line to the three points selected in the central region of the scaling regime on a log log plot.) We see that all the values are slightly larger than one and the value gets smaller as d/L becomes smaller. We expect that this effect for finite size of d/L may lead to the result of the exponent one in the small d/L limit as justified in Sec. 4.5, although further confirmation requires a separate study.

4. Theoretical interpretations

4.1. Maximum crack-tip stress on the lattice

In the static limit, the maximum stress that can appear at the crack tip is given by

$$\sigma_M \simeq \sigma_0 \left(\frac{L}{d} \right)^{\frac{1}{2}} \quad (5)$$

This is understood as follows. In the continuum limit, the stress distribution near the crack tip at the distance r from the tip is generally given by $\sigma(r) \simeq \sigma_0(L/r)^{1/2}$ when the crack size is larger than L [21]. This continuum expression no longer holds when r approaches a critical size below which the system cannot be regarded as a continuum system anymore. Since this critical scale is given by the lattice constant d , the maximum stress σ_M that appears at the crack tip

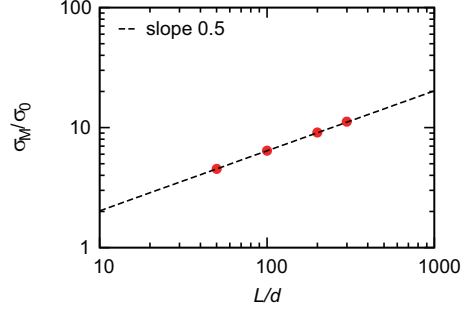


Fig. 5: The maximum stress at the crack tip in the present lattice model. The simulation data are well on the line with slope 1/2, which confirms Eq. (5).

may be given by Eq. (5). This naively expected relation [25] is confirmed by simulation in the present model as shown in Fig. 5.

4.2. Mechanism of crack propagation

130 As in Fig. 2(a), at the moment $t = t_n$, the force acting on the bond located at the crack tip ($i = n$), reaches the critical value f_c , the bond is broken. Just after this moment, the stress on the bond at the new crack tip ($i = n + 1$) has yet to reach the critical value and the stress on the tip starts to increase till the bond breaks at $f_c = \sigma_c d^2$. Note that this stress-increasing process is not
 135 instantaneous because of the finite relaxation time τ .

4.3. Lower and upper bounds for the scaling law

As seen below, the lower and upper bounds for the scaling law correspond to the conditions $\sigma_c < \sigma_M$ and $\sigma_0 < \sigma_c$, respectively. Equation (5) implies that, for a given σ_0 , a crack can propagate only if $\sigma_c < \sigma_M$, from which we obtain
 140 $G/G_0 = (\sigma_0/\sigma_c)^2 > (\sigma_0/\sigma_M)^2 \simeq d/L$: the lower bound is given by $d/L \simeq G/G_0$ as already given in Eq. (3). In contrast, in the limit $\sigma_0 = \sigma_c$, we expect the propagation speed diverges, because any stress concentration is not required for failure. This leads to the upper bound in Eq. (3), because $\sigma_0 = \sigma_c$ can be cast into the form $G/G_0 = 1$.

145 As indicated in the captions to Figs. 3 and 4, we find that the lower bounds
in all the cases are well described numerically by $G/G_0 = k_1 d/L$ with $k_1 = 2.4$,
which is consistent with the results shown in Fig. 5. The dashed line in Fig.
5 corresponds to $\sigma_M/\sigma_0 = k_2(L/d)^{1/2}$, i.e., $(\sigma_0/\sigma_M)^2 = (k_2)^{-2}d/L$, with $k_2 =$
0.64. Then, according to the argument in the previous paragraph, the lower
150 bound should be given by $G/G_0 = (k_2)^{-2}d/L$. This means $k_1 = (k_2)^{-2}$, which
holds well (2.4 is nearly equal to 0.64^{-2}).

4.4. Change in the shape of crack tip with speed

The change in the shape of crack tip with propagation speed, as shown
in Fig. 2(a), is understood as follows. When the propagation is slow, the
155 shape should become close to a static shape, namely, a parabolic shape [1,
2]. When the propagation is very fast near the limit $\varepsilon = \varepsilon_c$, the crack shape
is practically formed by two parallel lines (crack surfaces) separated by the
distance $\varepsilon_c d$ because bonds near the crack tip are broken almost simultaneously
without no time for relaxation, which suggests the sharpening of the crack shape
160 at large speeds. Note that when the crack speed is high, the relaxation of the
system continues after the passage of the crack tip.

4.5. Interpretation of the scaling regime

In a scaling regime, if exists, we expect a scaling form $V/V_0 \simeq (G/G_0)^\nu$
with the scaling exponent ν , considering the natural units V_0 and G_0 . When
165 the propagation speed is relatively slow, the released energy per time scaling
as GVd is consumed as the dissipation per time $\eta\dot{\varepsilon}^2 L^2 d$. In addition, we may
expect V scales with $\dot{\varepsilon}$, which implies $G \simeq V$, i.e., $\nu = 1$, in agreement with Eq.
(3).

5. Discussion

170 5.1. Previous results in accordance with present results

As shown above, the exponent for the scaling law is reasonably close to one.
This might correspond to some experimental observations, see for example [22]

or to very specific cases considered theoretically for example in Ref. [29], while in most of the cases examined in this paper, an exponent $1/2$ is predicted, as
175 observed experimentally in Ref. [23]. Note that different exponents have also been reported for various polymer-based materials (e.g. [4, 12, 30, 31])

As shown above, we observe that crack shape changes from a parabolic shape at high crack velocities. Our observation is in agreement with previous experiments and simulations, for example, in Refs. [32] and [33].

180 5.2. *Effect of inertia*

If we include the inertial effect, the propagation speed V may finally reach the speed of elastic wave (sound speed V_s). In such a case, the scaling regime would end or the second moderate jump (the second region in which relatively abrupt change in velocity is observed) would be cut off (depending on the size
185 of σ_c) at the corresponding energy release rate G_s above which the propagation speed V is nearly equal to the sound speed V_s irrespective of the value of energy release rate.

5.3. *Lower and upper bounds discussed in previous studies*

Surprisingly, the lower bound for the scaling regime that emerges from the
190 present model turns out to be physically the same with the one discussed in a classic theory, and thus the present model gives novel insight into the classic theory. We showed the lower bound is given by $G/G_0 = d/L$, which means that the energy release rate G approaches $E\varepsilon_c^2 d/2$ at the bound. In fact, this expression can be derived from a result of the classic theory by Lake and Thomas
195 [19] when d is identified with the cross linking distance in the case of rubbers, as suggested in Ref. [19] with the aide of the result obtained in Ref. [34]. Thus, the simple physical interpretation of the lower bound given in the present study elucidates an interesting physical meaning of the classic theory: the static fracture energy discussed by Lake and Thomas corresponds to the critical state
200 in which the maximum stress σ_M at the crack tip coincides with the intrinsic failure stress σ_c .

The upper bound for G is discussed, for example, in Ref. [24], by using a model with two characteristic moduli. The present study shows that even a simpler model with a single characteristic modulus possesses the upper bound
205 of different physical origin, which is more fundamental and model-independent. This implies that in a real system the least upper bound could be determined as a result of competition between these two types of upper bounds.

The present simple model suggests physical origins of the existence of two bounds for crack propagation: both bounds originate from stress concentration and the intrinsic failure strength σ_c . (1) The lower bound is understood from
210 stress concentration as explained in Sec. 4.3 by using Eq. (5) and Fig. 5 (The maximum stress σ_M should be larger than σ_c). (2) The upper bound G_0 is understood from no need for stress concentration by noting Eq. (4) (At the upper bound, no stress concentration is required for a crack to propagate
215 because the initial strain already reach the critical strain). Since the stress concentration and intrinsic fracture strength are model-independent concepts, our results imply a possibility that the upper and lower bounds could exist in other models from the same physical origins.

Our results would be useful not only for future fundamental studies but
220 also for future development of tough polymer-based materials. For example, one possible design principle for developing materials highly resistant for crack propagation would be making the value of the lower bound larger; in other words, the lower bound is a good marker for developing tough materials. This is because crack propagation does not occur below the lower bound and, thus, this
225 principle would guide us to reduce the risk of crack propagation in materials. Accordingly, an expression for the lower bound clarifying its dependence on important parameters could be useful and open the possibility for controlling the value of the lower bound, which is a good marker for developing tough materials.

230 **Acknowledgements**

The authors thank Dr. Katsuhiko Tsunoda and Yoshihiro Morishita (Bridgestone Corporation, Japan) for useful discussions. This research was partly supported by Grant-in-Aid for Scientific Research (A) (No. 24244066) of JSPS, Japan, and by ImPACT Program of Council for Science, Technology and Innovation (Cabinet Office, Government of Japan).

References

- [1] T. Anderson, *Fracture Mechanics* 3rd ed., CRC Press, Boca Raton, Florida, 2005.
- [2] B. Lawn, *Fracture of Brittle Solids*, 2nd ed., Cambridge Univ. Press, Cambridge, U.K., 1998.
- [3] A. Gent, J. Schultz, Effect of wetting liquids on the strength of adhesion of viscoelastic material, *J. Adhesion* 3 (4) (1972) 281–294.
- [4] A. Gent, Adhesion and strength of viscoelastic solids. is there a relationship between adhesion and bulk properties?, *Langmuir* 12 (19) (1996) 4492–4496.
- [5] M. K. Chaudhury, Rate-dependent fracture at adhesive interface, *J. Phys. Chem. B* 103 (31) (1999) 6562–6566.
- [6] Y. Morishita, H. Morita, D. Kaneko, M. Doi, Contact dynamics in the adhesion process between spherical polydimethylsiloxane rubber and glass substrate, *Langmuir* 24 (24) (2008) 14059–14065.
- [7] A. Kinloch, C. Lau, J. Williams, The peeling of flexible laminates, *Int. J. Fracture* 66 (1) (1994) 45–70.
- [8] R. Schapery, A theory of crack initiation and growth in viscoelastic media, *Int. J. Fracture* 11 (1) (1975) 141–159.

- 255 [9] J. Greenwood, K. Johnson, The mechanics of adhesion of viscoelastic solids, *Phil. Mag. A* 43 (3) (1981) 697–711.
- [10] M. Barber, J. Donley, J. Langer, Steady-state propagation of a crack in a viscoelastic strip, *Phys. Rev. A* 40 (1) (1989) 366.
- [11] B. Persson, E. Brener, Crack propagation in viscoelastic solids, *Phys. Rev. E* 71 (3) (2005) 036123.
- 260 [12] K. Tsunoda, J. Busfield, C. Davies, A. Thomas, Effect of materials variables on the tear behaviour of a non-crystallising elastomer, *J. Mater. Sci.* 35 (20) (2000) 5187–5198.
- [13] P. G. de Gennes, *C. R. Acad. Sci. Paris* 307 (1988) 1949.
- 265 [14] F. Saulnier, T. Ondarcuhu, A. Aradian, E. Raphaël, Adhesion between a viscoelastic material and a solid surface, *Macromolecules* 37 (3) (2004) 1067–1075.
- [15] Y. Kashima, K. Okumura, Fracture of soft foam solids: Interplay of visco- and plasto-elasticity, *ACS Macro Lett.* 3 (2014) 419–422.
- 270 [16] P. J. Petersan, R. D. Deegan, M. Marder, H. L. Swinney, Cracks in rubber under tension exceed the shear wave speed, *Phys. Rev. Lett.* 93 (1) (2004) 015504.
- [17] H. P. Zhang, J. Niemczura, G. Dennis, K. Ravi-Chandar, M. Marder, Toughening effect of strain-induced crystallites in natural rubber, *Phys. Rev. Lett.* 102 (2009) 245503.
- 275 [18] A. Livne, G. Cohen, J. Fineberg, Universality and hysteretic dynamics in rapid fracture, *Phys. Rev. Lett.* 94 (22) (2005) 224301.
- [19] G. Lake, A. Thomas, The strength of highly elastic materials, *Proc. Royal Soc. A* 300 (1460) (1967) 108–119.

- 280 [20] C. Y. Hui, Jagota A., S. J Bennisson, J. D. Londono, Crack blunting and the strength of soft elastic solids, *Proc. R. Soc. Lond. A* 459 (2003) 1489–1516
- [21] P. G. de Gennes, *Soft interfaces: the 1994 Dirac memorial lecture*, Cambridge Univ. Press, 2005.
- [22] T. Baumberger, C. Caroli, D. Martina, Fracture of a biopolymer gel as a
285 viscoplastic disentanglement process, *Eur. Phys. J. E* 21 (1) (2006) 81–89.
- [23] M. Lefranc, E. Bouchaud, Mode I fracture of a biopolymer gel: Rate-dependent dissipation and large deformations disentangled, *Extreme Mech. Lett.* 1 (2014) 97 – 103.
- [24] P. G. de Gennes, *Soft adhesives*, *Langmuir* 12 (19) (1996) 4497–4500.
- 290 [25] Y. Aoyanagi, K. Okumura, Crack-tip stress concentration and structure size in nonlinear structured materials, *J. Phys. Soc. Jpn.* 78 (3) (2009) 034402.
- [26] Y. Wang, P. Mora, Macroscopic elastic properties of regular lattices, *J. Mech. Phys. Solids.* 56 (12) (2008) 3459 – 3474.
- 295 [27] A. P. Jivkov, J. R. Yates, Elastic behaviour of a regular lattice for meso-scale modelling of solids, *Int. J. Solids Struct.* 49 (22) (2012) 3089 – 3099.
- [28] G. Lake, *Fracture mechanics and its application to failure in rubber articles*, *Rubber Chem. Tech.* 76 (3) (2003) 567–591.
- [29] E. Bouchbinder, E. A. Brener, Viscoelastic fracture of biological composites,
300 *J. Mech. Phys. Solids.* 59 (11) (2011) 2279 – 2293.
- [30] B. N. J. Persson, O. Albohr, G. Heinrich, H. Ueba, Crack propagation in rubber-like materials, *J. Phys. Cond. Matt.* 17 (44) (2005) R1071
- [31] C. Creton, M. Ciccotti, *Fracture and adhesion of soft materials: a review*, *Rep. Prog. Phys.* 79 (4) (2016) 046601

- 305 [32] R. Long, M. Lefranc, E. Bouchaud, C.-Y. Hui, Large deformation effect
in mode i crack opening displacement of an agar gel: A comparison of
experiment and theory, *Extreme Mech. Lett.* 9, Part 1 (2016) 66 – 73.
- [33] Y. Morishita, K. Tsunoda, K. Urayama, Crack-tip shape in the crack-
growth rate transition of filled elastomers, *Polymer* 108 (2017) 230 - 241.
- 310 [34] A. Thomas, Rupture of rubber. ii. the strain concentration at an incision,
J. Polym. Sci. 18 (88) (1955) 177–188.